Hindawi
Shock and Vibration
Volume 2020, Article ID 2052140, 12 pages
https://doi.org/10.1155/2020/2052140

Research Article

Modelling and Analysis of a Magnetorheological Damper with Nonmagnetized Passages in Piston and Minor Losses

Guojie Li and Ze-Biao Yang

School of Mechanical and Automotive Engineering, South China University of Technology, Guangzhou, China

Correspondence should be addressed to Guojie Li; ajiehx@163.com

Received 21 October 2019; Accepted 4 December 2019; Published 31 January 2020

Academic Editor: Miguel Neves

This work aims to establish the mathematical model with the high effectiveness in predicting the damping force of an MR damper with nonmagnetized passages in piston. The pressure drops due to viscous loss, MR effect, and the minor losses at the inlet and outlet of passages are considered in the mathematical model. The widely reported Bingham model is adopted to describe the mechanical property of MR fluid. The mechanical behaviours of the MR damper are experimentally evaluated under different excitations and current. The yield stress of MR fluid with respect to the current applied to piston coil is obtained by finite element analysis in Ansoft Maxwell 14.0. The proposed model is validated by comparing the simulated damping characteristics with the measured data under various currents applied to the piston coil. The simulated results are also compared with those obtained from the mathematical model without the pressure drop due to the minor losses at the inlet and outlet of passages. The comparisons show that the proposed mathematical model can yield more accurate predictions of damping force. This indicates that the pressure drop due to the minor losses is significant and nonnegligible. The nonlinearity of force-velocity characteristics is discussed. In order to quantitatively explain the necessity of taking the minor losses into account for modelling the MR damper, the proportion of pressure drop due to the minor losses to the total pressure drop is investigated and discussed. Pressure drops due to the minor losses and viscous loss are also investigated and discussed. At last, the proposed mathematical model is used to analyse the working principle of nonmagnetized passages.

1. Introduction

MR damper is the energy absorber with favorable performance based on the rheological property of MR fluid. The MR fluid is the smart material composed of micrometer-scale magnetic particles and carrier oil. After being applied magnetic field, MR fluid transforms to a solid-like paste with controllable yield stress in milliseconds from viscous fluid [1–6]. By changing the magnetic field intensity, it exhibits reversible and continuously tunable rheological properties.

Taking advantage of MR fluid's adjustable mechanical characteristics, the MR damper is controllable and widely used for vibration control. It has many advantages, such as continuous tunable damping force, compact structure, long-term stability, low energy consumption, simple electronics, and straight forward control and quick response. MR dampers have been utilized to attenuate vibration in automobile industry, aerospace, artificial limb, buildings and bridges, etc [7–10]. Especially in automobile industry, for many ground vehicles, such as Audi R8/TT, Ferrari 599GTB, Cadillac SRX/SLR/Seville/DTS/XTS, and Porsche 911, MR dampers have been developed and integrated in the suspension [11].

The MR damper with nonmagnetized passages in piston involved in this work is the latest developed for ground vehicles. It not only has the passage which can be magnetized but also has nonmagnetized passages in the middle of piston. The nonmagnetized passages will never be magnetized even when the electromagnetic coil is applied current. Relative to conventional MR dampers that only have a passage which can be magnetized, the MR damper with nonmagnetized passages improves the mechanical property [12, 13]. After

the magnetizable passage is magnetized, the MR fluid in it transforms to a solid-like paste. And the yield stress of MR fluid increases greatly. Thus, flow resistance is increased greatly. Then, the MR fluid is diverted and flows through the nonmagnetized passages. This MR damper, attributed to the nonmagnetized passages, results in a relatively much larger preyield-like region where the damping force gradually increases with piston velocity [14–19]. This MR damper with nonmagnetized passages in piston has been applied to vehicles. It helps vehicles achieve excellent riding comfort, handling characteristic, and road holding [18, 19].

Sohn et al. are the first to theoretically and systematically study the MR damper with nonmagnetized passages [19]. They formulated the analytical model for predicting the stroke load of the MR damper with nonmagnetized passages. The Bingham model was adopted. Viscous loss due to the viscosity of MR fluid was adopted. Viscous loss refers to the energy loss which results in pressure drop within passages. Numerical simulations for the damping forces are carried out. It was observed that the numerical errors of the simulated results are relatively large. The authors attributed it to the increased minor losses due to the abrupt change of section areas at the inlet and the outlet of passages. However, the minor losses are neglected in the mathematical model.

The minor losses refer to the energy losses which result in pressure drops at elbows and expansions, the abrupt change of section area at the inlet and the outlet, etc. Minor losses are generally neglected in long pipe systems [20, 21]. In the damper with shims added to the valve of the complex shape, and at high volumetric flow rates, due to the short length of the passages, the minor losses are significant and nonnegligible relative to viscous loss [15]. Wereley et al. indicated that for the MR damper without shims, it is necessary to take minor losses into account for predicting the damping force at high piston velocity (>1 m/s) when the MR damper is subjected to intense impacts, such as aircraft landing gear, crashworthy helicopter seat suspension systems, mine blast seat suspension systems, and gun recoil systems [21–25].

As most of research involving analytical models for predicting damper stroking load have focused on vibration isolation problems, where piston velocities remain low (≤1 m/s), these models typically neglect the minor losses [15, 21–23]. According to the study by Sohn et al., for the MR damper that was subjected to piston velocity lower than 1 m/s and without shims in piston of the simple shape, it may also be necessary to take the minor losses into account for the analytical model of the MR damper. However, neglecting the minor losses has been common way in establishing the analytical model for predicting MR damper stroking load.

This work aims to establish a mathematical model with high effectiveness for predicting the damping force of an MR damper with nonmagnetized passages in piston. Both viscous loss and minor losses are adopted in the proposed mathematical model. The widely reported Bingham model is adopted to describe the property of MR fluid. The yield stress of MR fluid with respect to the current applied to piston coil is obtained by an empirical equation and by the finite element analysis in Ansoft Maxwell 14.0. For comparison, the mathematical model without minor losses is established. Simulation reveals that the simulated results with the proposed model agree better with the measured damping force than those obtained from the mathematical without minor losses. It indicates that it is necessary to take minor losses into account for modelling the MR damper. In order to quantitatively explain the necessity of taking the minor losses at the inlet and outlet of passages into account for modelling of the MR damper, the proportion of pressure drop due to minor losses to the total pressure drop is investigated and discussed. Pressure drops due to viscous loss and minor losses are also investigated and discussed. The working principle of nonmagnetized passages is analysed using the proposed mathematical model.

2. Experimental Setup and Method

The schematic configuration of the automotive MR damper with nonmagnetized passages is shown in Figure 1. The length of the MR damper is L_{MAX} of 625 mm (extended) and L_{MIN} of 453 mm (compressed). The diameter of piston is D_P of 45.6 mm. The MTS370 system which is shown in Figure 2 is used to carry out the experimental test. Test conditions are listed in Table 1. The test is carried out under sinusoidal periodic excitation. The maximum velocity is 0.52 m/s. The current is applied to the piston electromagnetic coil. The current will generate heat and increase the MR damper's temperature. Therefore, the temperature of the MR damper is monitored by a thermal sensor.

3. Modelling of the MR Damper with Nonmagnetized Passages in Piston

3.1. Viscous Loss, Minor Losses, and the Loss due to MR Effect. The schematic configuration of the MR damper with nonmagnetized passages in piston is shown in Figure 1. When the MR fluid flows through the piston, it creates a pressure drop between the upper chamber and the lower chamber. The sources for pressure drops in piston are (1) the viscous loss due to viscous laminar flow of the MR fluid, (2) the minor losses due to the turbulent flow at the inlet and exit of passages, and (3) the loss due to MR effect.

3.1.1. Viscous Loss. The viscous loss is obtained using [19]

$$h_{\mathrm{vis.}} = f_{\mathrm{vis.}} \frac{L}{D} \frac{V^2}{2g}, \tag{1}$$

where $L, f_{\mathrm{vis.}}, D, V$, and g are the length of passage, coefficient of viscous loss, hydraulic diameter of passage, average flow velocity in passage, and the gravity acceleration, respectively.

Pressure drop due to viscous loss can be written as

$$\Delta P_{\mathrm{vis.}} = \rho g h_{\mathrm{vis.}}, \tag{2}$$

where ρ is the density of the MR fluid.

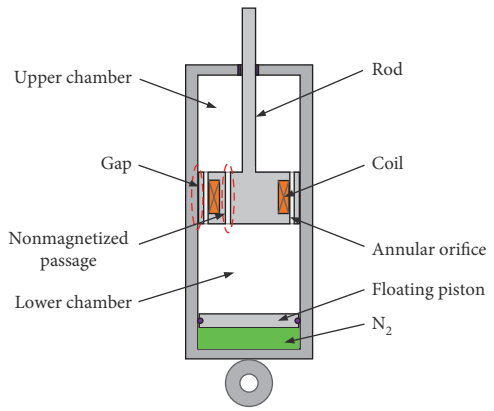

Figure 1: Schematic configuration of the MR damper with nonmagnetized passages in piston.

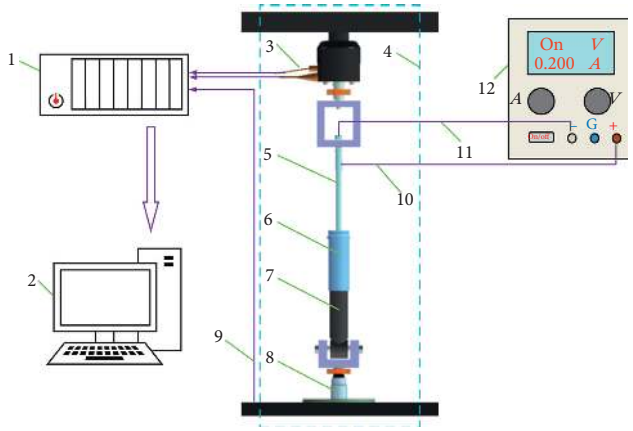

1-Data-acquisition system
2-PC
3-The force sensor
4-MTS370
5-Rod
6-Aluminum shell
7-Cylinder of MR damper
8-MTS370 actuator
9-The inner displacement sensor
10-Rod (connected to anode of current source)
11-Copper needle in rod (connected to cathode of current source)
12-Current source (Qiujing QJ3005T)

(a)

(b)

Figure 2: (a) Schematic of the experimental setup. 1, data acquisition system; 2, PC; 3, the force sensor; 4, MTS370; 5, rod; 6, aluminum shell; 7, cylinder of MR damper; 8, MTS370 actuator; 9, the inner displacement sensor; 10, rod (connected to anode of current source); 11, copper needle in rod (connected to cathode of current source); 12, current source (Qiujing QJ3005T). (b) Test rig.

Table 1: Test conditions.

Temperature	43 ± 2°C
Applied currents	0 A, 0.6 A, 1 A, 1.6 A, 2 A, 2.5 A
Frequency	3.3 Hz
Displacement	±25 mm

3.1.2. Minor Losses. The minor losses are considered as much smaller relative to viscous loss in long pipe systems. Therefore, the minor losses can be neglected in long piping systems. However, for the MR damper, even if the piston is of the simple shape, minor losses may not be negligible relative to viscous loss [19]. However, neglecting the minor losses and taking the first and the third source into account for pressure drop in passages has been the common way [15, 21–23]. In this work, the minor losses are involved in the mathematical model of the MR damper.

The minor losses are obtained using [15]

$$h_{\text{minor}} = \varepsilon \frac{V^2}{2g}, \tag{3}$$

where V, g, and ε are the average flow velocity in passage, gravity acceleration, and the coefficient of minor losses, respectively. ε is obtained from the experimental results and remains constant for all flow velocities [15].

The pressure drop due to minor losses can be written as

$$\Delta P_{\text{minor}} = \rho g h_{\text{minor}}. \quad (4)$$

3.1.3. The Loss due to MR Effect. The loss due to MR effect is obtained using

$$h_{\text{MR}} = \frac{\Delta P_{\text{MR}}}{\rho g}, \quad (5)$$

where ΔP_{MR} is the pressure drop caused by the MR effect.

3.2. Magnetic Properties of MR Fluid in the MR Damper. The Bingham model is adopted for the MR fluid. The Bingham model has been widely reported to describe characteristics of MR fluid for its simple form and effectiveness.

The Bingham model is expressed by

$$\tau_y(H) = \tau_0(H) \cdot \text{sign}(\dot{\gamma}) + \mu\dot{\gamma}, \quad (6)$$

where $\tau_0(H)$ is the yield shear stress generated by MR effect, H is the magnetic field intensity, μ is the dynamic viscosity, and $\dot{\gamma}$ is the shear rate. The dynamic viscosity μ can be measured by a rheometer Brookfield RST-CPS from Brookfield Corporation. The yield shear stress $\tau_0(H)$ can be calculated as follows.

The density of the MR fluid in the MR damper with nonmagnetized passages in piston is 2.63 g/ml which is higher than 2.38 g/ml of the MR fluid MRF122EG from the Lord corporation and lower than 3.05 g/ml of the MR fluid MRF132DG [26]. It indicates that the volume percentage of magnetic particles in the MR fluid in the MR damper differs from the MR fluid MRF122EG and MRF132DG. The yield stress with respect to the magnetic field intensity can be obtained using Dr. Dave's empirical equation [27]:

$$\tau_0(H) = 2.717 \times 10^5 C \varnothing^{1.5239} \tanh\left(6.33 \times 10^{-6} H\right), \quad (7)$$

where $\varnothing$ is the volume percentage of magnetic particles which can be derived from the density of each MR fluid, the density of carbonyl iron particles (7.86 g/cm^3), and the density of carrier oil (0.89 g/ml). The density of carrier oil is measured from the clear supernatant liquid of the settled and stratified MR fluid. The values of $\varnothing$ for MRF122EG, MRF132DG, and the MR fluid in the damper with non-magnetized passages are 21.4%, 31%, and 25%, respectively. C is a constant correlated with carrier oil. C varies for different carrier oil. H is the magnetic field intensity. The constant C is assumed as 0.686 and confirmed by the technical data of the MR fluid MRF122EG and MRF132DG as shown in Figures 3 and 4.

Using the confirmed constant C and the empirical equation (7), the yield stress of the MR fluid in the damper with nonmagnetized passages in piston with respect to the magnetic field intensity can be obtained. It is given in Figure 5.

In order to obtain the yield stress with respect to the current applied to the piston coil, the magnetic field intensity with respect to the current applied to the piston coil is needed.

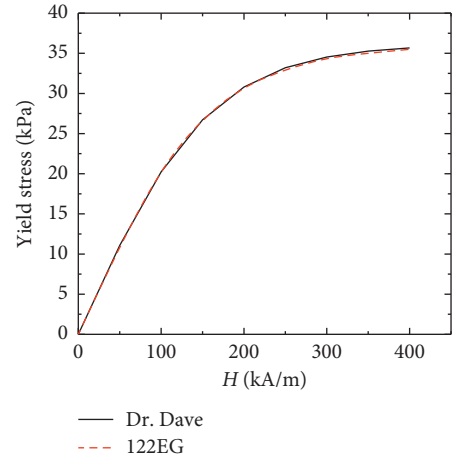

Figure 3: Technical data of MRF 122EG from Lord and the simulated result with Dr. Dave's empirical formula.

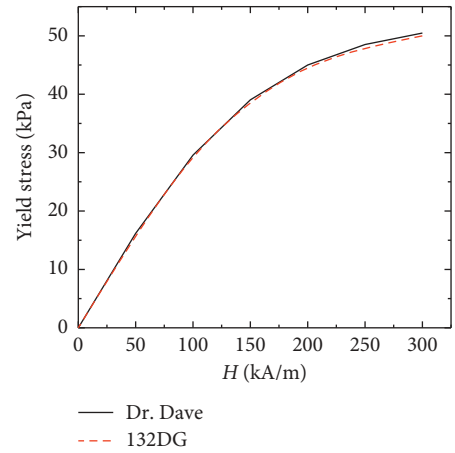

Figure 4: Technical data of MRF 132DG from Lord and the simulated result with Dr. Dave's empirical formula.

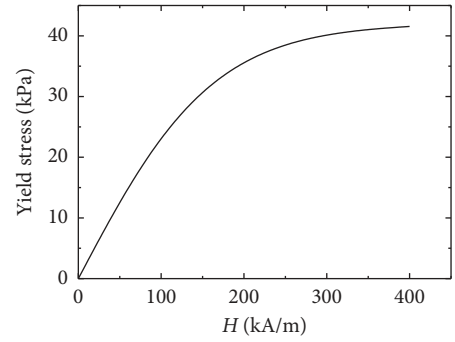

Figure 5: The simulated yield stress of MR fluid with Dr. Dave's empirical formula.

The magnetic simulation for piston and cylinder is performed in Ansoft Maxwell 14.0. 2D model is established. The structure and materials of piston are shown in Figures 6 and 7.

Settings in Ansoft Maxwell 14.0 are given in Table 2. Magnetic field intensity distribution is shown in Figure 7.

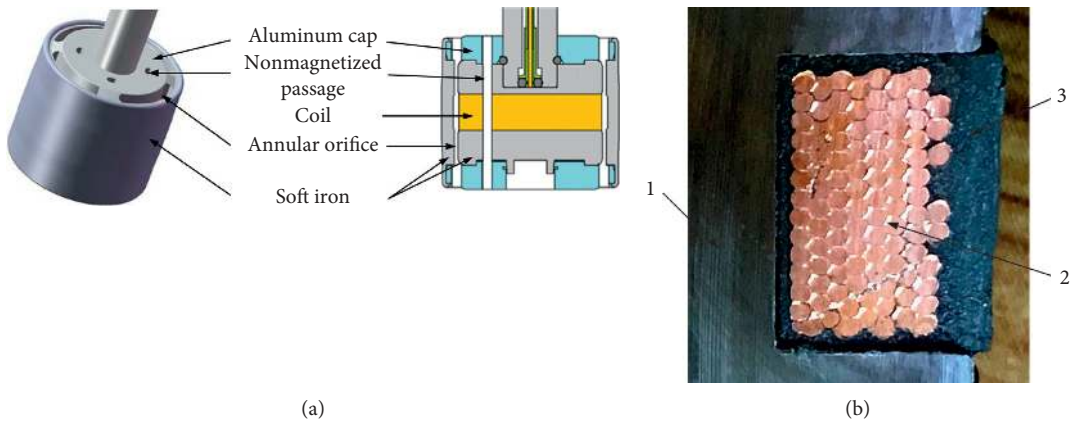

Figure 6: Configuration of the piston. (a) The piston with three nonmagnetized passages. (b) The coil: 1, steel 1008; 2, copper; 3, polyester (P.S.: cylinder-steel 1008). 1, the soft iron parts of piston; 2, the aluminum caps of piston; 3, coil; 4, annular orifice; 5, cylinder of soft iron.

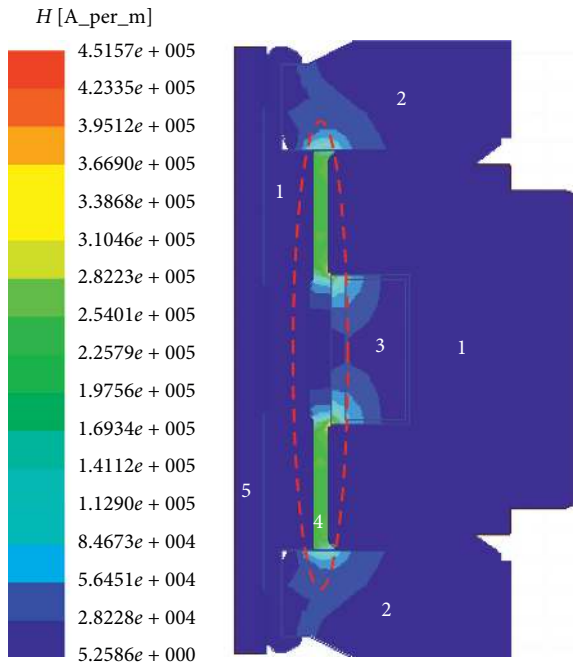

Figure 7: The distribution of magnetic field intensity in section of piston when current of 2.5 amperes is applied.

Table 2: Settings of magnetic simulation in Ansoft Maxwell 14.0.

Settings	Value
Boundary	Balloon
Current	Positive
Maximum length of elements	Length-0.2 m
Maximum number of elements	1000
Restrict length of elements	Yes
Maximum number of passes	10
Percent error	1
Solve matrix	After last pass
Others	Default

The simulated magnetic field intensity with respect to the current is shown in Figure 8. For the current 0 A, 0.6 A, 1 A, 1.6 A, 2 A, and 2.5 A, the magnetic field intensity is 0 kA/m, 24 kA/m, 49 kA/m, 82 kA/m, 116 kA/m, and 154 kA/m, respectively. Then, from Figure 5, the yield stresses at the magnetic field intensities 0 kA/m, 24 kA/m, 49 kA/m, 82 kA/m, 116 kA/m, and 154 kA/m can be obtained as 0 kPa, 6.1 kPa, 12.5 kPa, 20 kPa, 27 kPa, and 30 kPa, respectively. However, the authors consider there is residual magnetic field in the piston. And the yield stress at the current 0A is given as 1.2 kPa. The discussion is given in Section 4.2.

Combining Figures 5 and 8 yields Figure 9. One can find the yield stress at any current in Figure 9.

3.3. Mathematical Model. When the piston, as shown in Figure 6, moves back and forth in cylinder of MR damper, there are fluid flows in each passage, including the gap between piston and cylinder as shown in Figure 1. The MR fluid works on flow mode which is shown in Figure 10. Here, assume the laminar flow and turbulent flow arises in region A and region B, respectively. Both the minor losses and the viscous loss are taken into account for establishing the mathematical model.

The proposed mathematical model of the damping force is given as

$$F_d = F_{\text{vis.}} + F_{\text{minor}} + F_{\text{MR}} + F_{\text{fri.}}, \tag{8}$$

where $F_{\text{vis.}}, F_{\text{minor}}, F_{\text{MR}}$, and $F_{\text{fri.}}$ are the damping force generated by viscous loss due to laminar viscous flow, minor losses due to turbulent flow, loss due to MR effect, and seal friction respectively. When the piston moves in the cylinder at the very low velocity of 0.1 mm/s, $F_{\text{fri.}}$ is obtained as 37 N by measurement. $F_{\text{vis.}}, F_{\text{minor}}$, and F_{MR} are defined by $F_{\text{vis.}} = (A_p - A_r)h_{\text{vis.}}$, $F_{\text{minor}} = (A_p - A_r)h_{\text{minor}}$, and $F_{\text{MR}} = (A_p - A_r)\, h_{\text{MR}}$, respectively. The definition of $F_{\text{vis.}}, F_{\text{minor}}$, and F_{MR} in formula (8) is only used to explain the components of damping force. The damping force F_d will be obtained by solving simultaneous equations (12)–(14), (17), (19), (21), and (22) which will be given below, without solving $F_{\text{vis.}}, F_{\text{minor}}$, and F_{MR}, respectively. As the nitrogen

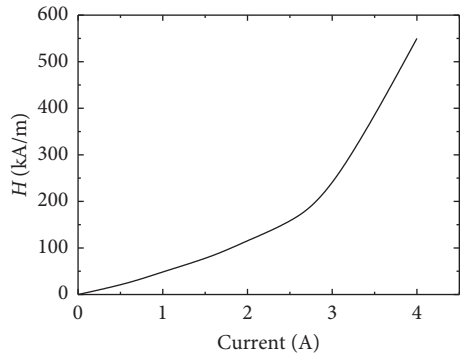

Figure 8: The simulated magnetic field intensity in annular orifice with respect to the current applied to piston.

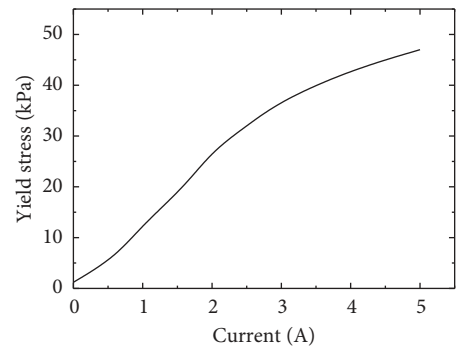

Figure 9: The yield stress of MR fluid with respect to the current applied to piston.

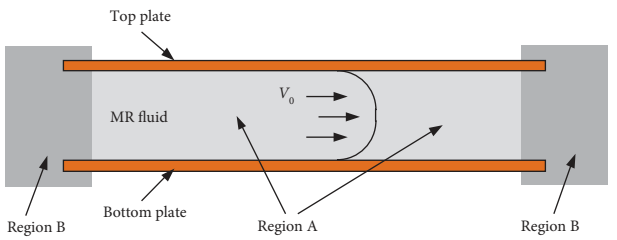

Figure 10: Schematic of flow mode with region A: laminar flow (the part away from the inlet and outlet) and region B: turbulent flow (the inlet and the outlet of each passage).

accumulator of the MR damper produces an effect similar to that of an elastic element, the elastic force due to the nitrogen accumulator is not included in damping force.

Four assumptions are made to model the damping force of the MR damper:

(1) The MR fluid cannot be compressed

(2) In the region A of each passage in piston, there is the stable laminar flow

(3) In the region B of each passage in piston, there is the turbulent flow

(4) There are same pressure drops in each passage

The motion of MR fluid in passages is governed by the Euler equation:

$$\frac{P_2}{\rho g} + \frac{V_2^2}{2g} + z_2 = \frac{P_1}{\rho g} + \frac{V_1^2}{2g} + z_1 + h, \tag{9}$$

where ρ, g, and h are the density of MR fluid, the acceleration of gravity, and total loss, respectively. P_1 and V_1 are the pressure and average flow velocity in the lower chamber, respectively. P_2 and V_2 are the pressure and average flow velocity in the upper chamber, respectively. z_1 and z_2 are the heights of fluid in each chamber.

For the incompressibility of MR fluid and the consistent section area of the flow passage, the average flow velocities in each chamber are the same:

$$V_1 = V_2. \tag{10}$$

The heights of fluid in each chamber are approximately equal. It can be expressed as

$$z_1 - z_2 \approx 0. \tag{11}$$

Then formula (9) can be rewritten as

$$\Delta P = P_2 - P_1 = \rho g h. \tag{12}$$

The damping force is written in the following form [19]:

$$F_d = \left(A_p - A_r\right)\Delta P, \tag{13}$$

where A_p is the section area of piston and A_r is the section area of rod.

The total loss in the annular orifice is written in the following form:

$$h_{\text{ori.}} = f_{\text{ori.}} \frac{L_{\text{ori.}}}{D_{\text{ori.}}} \frac{V_{\text{ori.}}^2}{2g} + \varepsilon \frac{V_{\text{ori.}}^2}{2g} + \frac{\Delta P_{\text{MR}}}{\rho R}, \tag{14}$$

where ΔP_{MR} is the pressure drop in the annular orifice caused by MR effect. $L_{\text{ori.}}$, $D_{\text{ori.}}$, $f_{\text{ori.}}$, ε, and $V_{\text{ori.}}$ are the length, hydraulic diameter, the coefficient of viscous loss, the coefficient of minor losses, and average flow velocity, respectively. ΔP_{MR} is given in formula (24).

$f_{\text{ori.}}$ can be written in the following form:

$$f_{\text{ori.}} = \frac{96}{\text{Re}} = \frac{96\mu}{\rho V_{\text{ori}} D_{\text{ori}}}, \tag{15}$$

where Re is the Reynolds number and μ is the dynamic viscosity.

The annular orifice can be considered as the duct structure of two parallel plates as shown in Figure 10. The width of the parallel plates, W, is much larger than the distance d_{ori}. Therefore, the width W can be assumed as infinite. Then the hydraulic diameter can be expressed as follows:

$$D_{\text{ori.}} = \frac{4W d_{\text{ori.}}}{2d_{\text{ori.}} + 2W} = 2d_{\text{ori.}}. \tag{16}$$

The total loss in the nonmagnetized passages can be given by

$$h_{\text{nmp.}} = f_{\text{nmp.}} \frac{L_{\text{nmp.}}}{D_{\text{nmp.}}} \frac{V_{\text{nmp.}}^2}{2g} + \varepsilon \frac{V_{\text{nmp.}}^2}{2g}, \tag{17}$$

where $L_{\text{nmp.}}$, $f_{\text{nmp.}}$, $D_{\text{nmp.}}$, and $V_{\text{nmp.}}$ are the length, the coefficient of viscous loss, hydraulic diameter, and average

flow velocity in nonmagnetized passages, respectively. $D_{\text{nmp.}} = d_{\text{nmp.}}$. Here $d_{\text{nmp.}}$ is the diameter of the nonmagnetized passages. The coefficient of viscous loss is written in the following form:

$$f_{\text{nmp.}} = \frac{64}{\text{Re}} = \frac{64\mu}{\rho V_{\text{nmp.}} D_{\text{nmp.}}}. \tag{18}$$

The gap between the piston and the cylinder is also considered as a duct structure of two parallel plates. The losses in gap are expressed as follows:

$$h_{\text{gap}} = f_{\text{gap}} \frac{L_{\text{gap}}}{D_{\text{gap}}} \frac{V_{\text{gap}}^2}{2g} + \varepsilon \frac{V_{\text{gap}}^2}{2g}, \tag{19}$$

where $L_{\text{gap}}, f_{\text{gap}}, D_{\text{gap}}$, and V_{gap} are the length, the coefficient of viscous loss, hydraulic diameter, and average flow velocity, respectively. $D_{\text{gap}} = 2d_{\text{gap}}$. Here d_{gap}. is the width. The coefficient of viscous loss is written in the following form:

$$f_{\text{gap}} = \frac{96}{\text{Re}} = \frac{96\mu}{\rho V_{\text{gap}} D_{\text{gap}}}. \tag{20}$$

According to assumption (4), total losses in each passage are the same:

$$h_{\text{ori.}} = h_{\text{nmp.}} = h_{\text{gap}}. \tag{21}$$

Velocities in each passage satisfy

$$V_{\text{pist.}}\left(A_p - A_r\right) = V_{\text{ori.}} A_{\text{ori.}} + nV_{\text{nmp.}} A_{\text{nmp.}} + V_{\text{gap}} A_{\text{gap}}, \tag{22}$$

where $V_{\text{pist.}}$ is the velocity of the piston, $A_{\text{ori.}}$, $A_{\text{nmp.}}$, and A_{gap} are the section area in each passage, and n is the number of nonmagnetized passages. The pressure drop in piston due to the MR effect is written in the following form [19]:

$$\Delta P_{\text{MR}} = \frac{cL_{\text{ori.}}}{d} \tau_y(H), \tag{23}$$

where c is the coefficient of the flow velocity and $\tau_y(H)$ is the total yield shear stress which is a function of magnetic field intensity.

Combining (14), (17), (19), (21), and (22) yields $V_{\text{ori.}}$, $V_{\text{nmp.}}$, and V_{gap}. Substituting $V_{\text{ori.}}$, $V_{\text{nmp.}}$, and V_{gap} into formula (14) gives $h_{\text{nmp.}}$. According to assumption (4), substituting $h_{\text{nmp.}}$ into formula (12) yields ΔP. Then, substituting ΔP into formula (13), the damping force of MR damper will be obtained. The parameters used in simulation are listed in Table 3. The calculation is performed in Matlab R2014a.

Table 3: The parameters used in modelling the MR damper.

Parameters	Values
$d_{\text{nmp.}}$ (m)	3.9×10^{-4}
$d_{\text{ori.}}$ (m)	7×10^{-4}
d_{gap} (m)	2×10^{-4}
$L_{\text{ori.}}$ (m)	0.017
ρ (kg/m^3)	2950
A_r (m^2)	1.5394×10^{-4}
A_p (m^2)	1.7×10^{-3}
$A_{\text{nmp.}}$ (m^2)	3.1416×10^{-6}
A_{gap} (m^2)	2.8965×10^{-5}
L_{MAX} (mm)	625
L_{MIN} (mm)	453
D_P (mm)	45.6
μ	0.03
g (m/s^2)	9.8
ε	0.7
$A_{\text{ori.}}$ (m^2)	1.2032×10^{-4}
L_{gap} (m)	0.0387
c	1.4
τ_0 at 2.5 amperes	30 kPa
τ_0 at 2 amperes	27 kPa
τ_0 at 1.6 amperes	20 kPa
τ_0 at 1 ampere	12.5 kPa
τ_0 at 0.6 ampere	6.1 kPa
τ_0 at 0 ampere	1.2 kPa

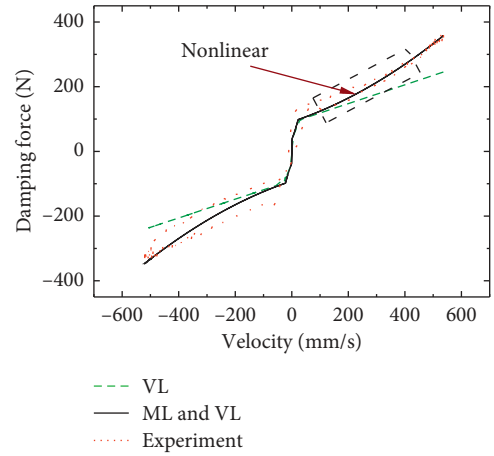

Figure 11: Comparison between simulated results and measured data at zero amperes (VL: viscous loss; ML: minor losses).

4. Simulation Results and Discussion

4.1. Simulation Results. The simulated results from the mathematical model adopting both minor losses and viscous loss (ML&VL) are compared with those simulated damping forces without minor losses (ML) in Figures 11–16. Also, the simulated results are compared with measured results. Relative errors (Re) and average relative errors ($\overline{\text{Re}}$) are listed in Tables 4 and 5, respectively. The errors between the simulated and measured results are used to evaluate the performance of the mathematical model. Re is expressed as

$$\text{Re} = \left| \frac{F_{\text{sim.}i} - F_{\text{exp.}i}}{F_{\text{exp.}i}} \right|, \tag{24}$$

where $F_{\text{sim.}i}$ and $F_{\text{exp.}i}$ are the ith simulated damping force and measured damping force in experiment, respectively. The average relative error ($\overline{\text{Re}}$) is expressed as

$$\overline{\text{Re}} = \frac{1}{m} \sum_{i=1}^{m} \left| \frac{F_{\text{sim.}i} - F_{\text{exp.}i}}{F_{\text{exp.}i}} \right|, \tag{25}$$

where m represents the number of data points.

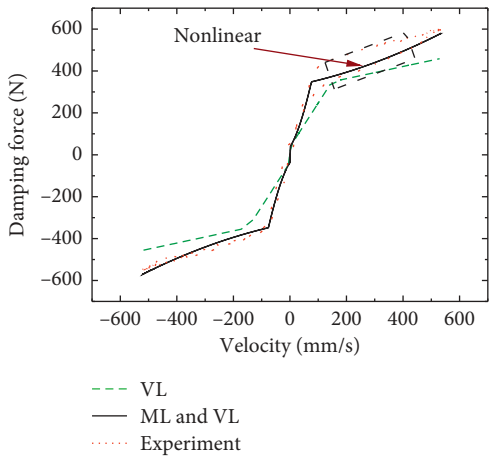

Figure 12: Comparison between simulated results and measured data at 0.6 ampere (VL: viscous loss; ML: minor losses).

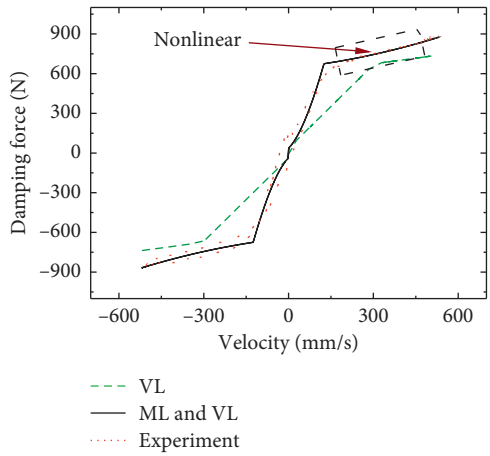

Figure 13: Comparison between simulated results and measured data at 1 ampere (VL: viscous loss; ML: minor losses).

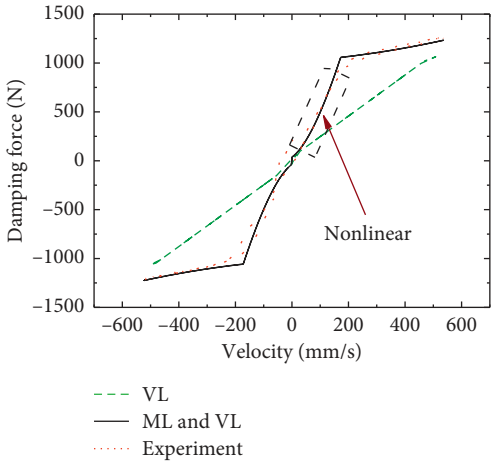

Figure 14: Comparison between simulated results and measured data at 1.6 amperes (VL: viscous loss; ML: minor losses).

4.2. Discussion. The force at knee points of the curve of experiment in Figure 11 is about 100 N (around 50 mm/s) which is larger than the friction force 37 N (0.1 mm/s). It is thought that when piston moves at the very low velocity of 0.1 mm/s, the pressure drop in piston is negligible. MR fluid only passes in the nonmagnetized passages because the magnetizable passage (the annular orifice) is magnetized by the small residual magnetic field in piston and the MR fluid in it transforms to a solid-like paste. When piston moves at the velocity of about 50 mm/s, the pressure drop in piston is nonnegligible and big enough to overcome the yield stress of MR fluid in the magnetizable passage. Then the MR fluid begins to pass in both magnetizable passage and the nonmagnetized passages. This yields the knee points shown in the curve of experiment in Figure 11. Using the least squares method, the residual magnetic field at current of zero amperes $\tau_0 (I = 0\,\text{A})$ is obtained as 1.2 kPa.

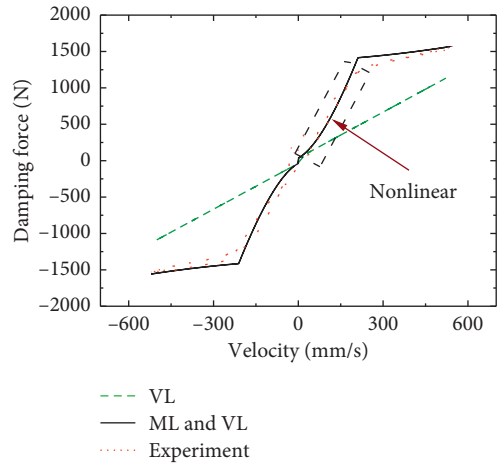

Figure 15: Comparison between simulated results and measured data at 2 amperes (VL: viscous loss; ML: minor losses).

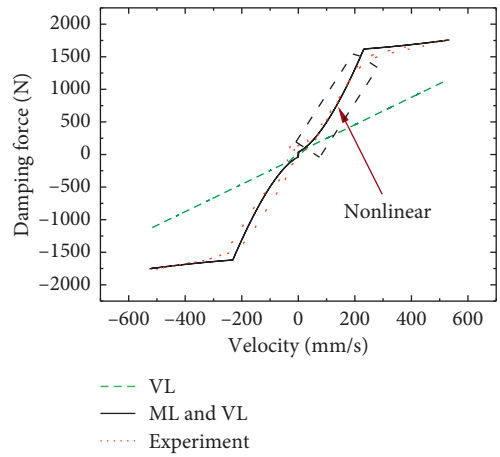

Figure 16: Comparison between simulated results and measured data at 2.5 amperes (VL: viscous loss; ML: minor losses).

The simulated results are compared with the measured damping forces in Figures 11–16. Simulated results at each current obtained from the mathematical model adopting both minor losses and viscous loss reveal excellent agreement with the measured data. The simulated results obtained from the mathematical model without minor losses are relatively smaller than the measured results. It proves the

Table 4: Relative errors between the measured data and the simulated results at the current of 2 amperes.

Piston velocity (mm/s)	ML&VL (%)	VL (%)
50	8	26.7
100	12.9	57
300	6.3	51
500	0.9	29.1

Table 5: The average relative errors between the measured data and the simulated results.

Current (A)	ML&VL (%)	VL (%)
0	23.6	30.3
0.6	50.8	62.6
1	11.7	26.4
1.6	17.7	40.6
2	12.3	46.2
2.5	13.8	53.9

minor losses due to the abrupt change of section areas at the inlet and the outlet of each passage are significant. It also indicates that the minor losses are needed in modelling the MR damper.

The relative errors between the measured data and the simulated results are listed in Tables 4 and 5. It is found that, in general, the high velocity and high current help the MR damper lower the errors. An MR damper, when it is applied large current or subjected to excitation of high velocity, will yield the large damping forces. However, for the MTS370, the measurement errors remain the same. It is thought that the measurement errors have less effect on the measured results when the MR damper has the large damping force.

On the other hand, it is obvious that the experimental force-velocity curves in Figures 11–16 are all nonlinear. The minor losses are the nonlinear quadratic function of flow velocity while the viscous loss due to laminar flow is linear with the flow velocity. The nonlinearity in force-velocity curves in Figures 11–16 proves that minor losses exist and cannot be ignored. The authors observe that the nonlinearity exists in all areas of the force-velocity curves even if more pronounced in some. The black (dashed) boxes show some of these areas. Also, a discussion on the existence of nonlinearity (refer to minor losses) in all areas is given below.

In order to quantitatively explain the necessity of taking the minor losses into account for predicting the stroke load of MR damper, the proportions of pressure drop due to minor losses to the total pressure drop at no current and current of 2 amperes are given in Figure 17. Both curves indicate the proportion of pressure drop due to minor losses increases dramatically after the piston begins to move. For no current, when piston velocity reaches 21.8 mm/s, the proportion reaches 14.6%. Then, the annular orifice changes from blocked-up state into fully open state. The proportion continues to increase rapidly and reaches 47% at last. For 2 amperes, when piston velocity reaches 212 mm/s, the proportion of pressure drop due to minor losses reaches 71%. Then, the proportion reaches 73% at last. It indicates that the

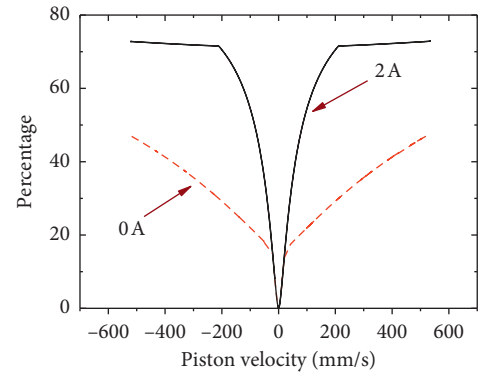

Figure 17: The proportions of pressure drops due to minor losses to the total pressure drop.

minor losses due to the turbulent flow at the inlet and outlet of each passage in piston are significant and should not be neglected even when the MR damper is subjected to the excitation of very low velocity. Therefore, the mathematical model adopting both minor losses and viscous loss is of much higher effectiveness for predicting the stroke load of MR damper.

The pressure drops due to viscous loss and minor losses in piston are investigated and given in Figure 18. Pressure drop due to viscous loss is linear with the flow velocity while that of minor losses is nonlinear. In the two figures, pressure drop due to viscous loss is larger than that of minor losses at low piston velocity while smaller at high piston velocity. Literatures [21–25] indicate that it is necessary to take minor losses into account for predicting the damping force at high piston velocity (>1 m/s). From Figure 18(b), it can be found that when the current in piston electromagnetic coil is 2 amperes, the pressure drop due to minor losses is larger than that due to viscous loss even at 0.069 m/s. It explains the nonlinearity of force-velocity curves at very low piston velocity in Figures 11–16. And it proves that it is necessary to take minor losses into account for predicting the damping force even at the piston velocity lower than 0.069 m/s.

4.3. Application of the Proposed Mathematical Model to the Analysis of Annular Orifice-Nonmagnetized Passages Coupling. The MR damper with nonmagnetized passages in piston yields the minimal damping force when piston moves near the zero velocity. Before the knee point, the slope of damping force is reduced much relative to the conventional MR damper without nonmagnetized passages. Thus, the damping forces with gentle slope are obtained. Behind the knee point, the damping force increases much more slowly. For the force-velocity curves of 0 A, 1 A, and 2 A, the velocity that the knee point is located at enlarges from 0.05 m/s to 0.22 m/s. Velocities of knee points increase along with the applied current.

The phenomenon stated above is thought as a result of the annular orifice-nonmagnetized passages coupling. When the annular orifice is magnetized, the MR fluid transforms to a solid-like paste. Before the knee point, the MR fluid stops flowing in the annular orifice. Then, the MR fluid only flows

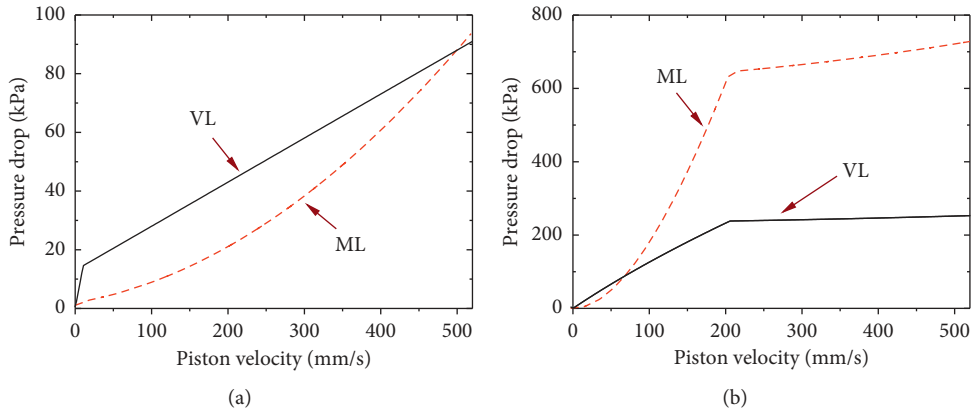

Figure 18: Pressure drops due to viscous loss (VL) and minor losses (ML), respectively. (a) 0 amperes. (b) 2 amperes.

in nonmagnetized passages. As the MR fluid can flow through the nonmagnetized passages freely, the MR damper yields the minimal damping force when the piston moves near the zero velocity. Attributed to the nonmagnetized passages, before the knee point, the slope of damping force is much lower relative to the conventional MR damper. At the knee point, the pressure drop in the annular orifice is so large that it overcomes the yield stress of MR fluid and the flow velocity in the piston annular orifice is increased from zero to high. As the annular orifice has the largest section area in passages, the total section area of passages is enlarged much. Thus, the increase of flow velocity slows down. Then, the increase of damping force due to viscosity slows down. As shown in Figures 11–16, the damping force has a much lower slope behind the knee points.

The mathematical model adopting both minor losses and viscous loss is of high effectiveness in predicting the stroke load of the MR damper. The application of this mathematical model to the quantitative analysis of annular orifice-nonmagnetized passages coupling is given as follows.

Using the proposed mathematical model, the flow velocity of MR fluid in each passage of piston can be simulated precisely. The simulated nominal velocities and absolute velocities in each passage are given in Figures 19 and 20, respectively.

Here, we define the nominal velocity in each passage as follows:

$$\mathrm{NV} = \frac{V}{\mathrm{Max}V_{\mathrm{nmp.}}}, \tag{26}$$

where $\mathrm{Max}V_{\mathrm{nmp.}}$ is the maximum $V_{\mathrm{nmp.}}$ and V is $V_{\mathrm{nmp.}}$, $V_{\mathrm{ori.}}$, or V_{gap}. NV is the ratio of V to $\mathrm{Max}V_{\mathrm{nmp.}}$.

Figure 19 indicates that the nominal velocity in gap $\mathrm{NV}_{\mathrm{gap}}$ enlarges along with the nominal velocity $\mathrm{NV}_{\mathrm{nmp.}}$ in nonmagnetized passages. And the nominal velocity in the annular orifice $\mathrm{NV}_{\mathrm{ori.}}$ is very close to zero when $\mathrm{NV}_{\mathrm{nmp.}}$ is between 0 and the value 0.41. The nominal velocity $\mathrm{NV}_{\mathrm{ori.}}$ and $\mathrm{NV}_{\mathrm{gap}}$ are both much smaller than the nominal velocity $\mathrm{NV}_{\mathrm{nmp.}}$. It indicates that when the annular orifice is magnetized, MR fluid only flows through the nonmagnetized passages and gap. And MR fluid mainly flows through the

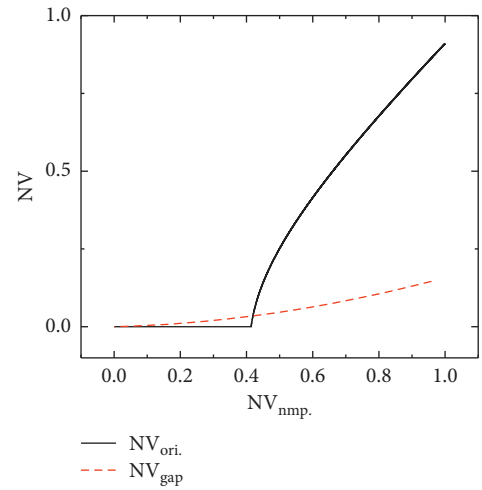

Figure 19: The simulated nominal velocities in passages at 2 amperes.

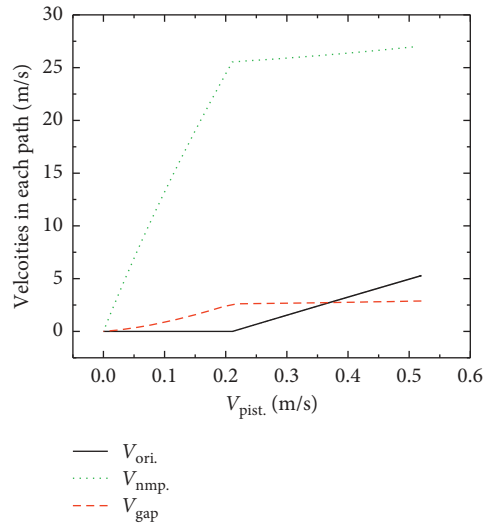

Figure 20: Velocities in passages vs. piston velocity at 2 amperes.

nonmagnetized passages. The nominal velocity $\mathrm{NV}_{\mathrm{ori.}}$ in annular orifice increases sharply once the nominal velocity $\mathrm{NV}_{\mathrm{nmp.}}$ reaches 0.41. The pressure drop in annular orifice is

so large that it overcomes the yield stress of fluid. As a result, the annular orifice allows the MR fluid to flow. Since the annular orifice is of the largest section area, it becomes the main passage of flow instead of nonmagnetized passages. As a result of much larger total section area of passages, the increase of damping force slows down. Therefore, Figure 19 explains the knee point and the linearity of the damping force at low piston velocity.

It is obvious that the nominal velocity $NV_{ori.}$ in Figure 19 yields a distortion when $NV_{nmp.}$ reaches 0.41. It is a result of the discontinuity of the Bingham model in preyield region. The distortion indicates that the flow of MR fluid at low excitation velocity occurs only in the piston nonmagnetized passages. However, in fact, there is the small amount of flow in the orifice in experiment [19]. Therefore, the simulated damping force has the largest errors at the knee points as shown in Figures 11–16.

Same conclusions can be drawn from Figure 20. And it is also convenient to find that there is the knee point where the increase of velocity in nonmagnetized passages which is the maximal one in the three velocities slows down. As the pressure drop due to minor losses is a quadratic function of flow velocity, the increase of proportion of pressure drop due to minor losses to the total pressure drop slows down as shown in Figure 17.

5. Conclusions

(1) The measured damping force shows nonlinearity as shown in Figures 11–16. It is the result of minor losses.

(2) Errors of simulated damping force adopting both viscous loss and minor losses were much smaller than that adopting only viscous loss. It is necessary to take minor losses into account for modelling of MR damper.

(3) The mathematical model adopting both viscous loss and the minor losses is of much higher effectiveness in predicting the stroke load of the MR damper than that without minor losses, even if the piston moves at the piston velocity even lower than 0.069 m/s.

(4) Using the proposed mathematical model, the annular orifice-nonmagnetized passages coupling was investigated and quantitatively analysed. It is the nonmagnetized passages that result in the knee points and the gentle slope of damping force in force-velocity curves.

Data Availability

The data used to support the findings of this study are available from the corresponding author upon request.

Conflicts of Interest

The authors declare that there are no conflicts of interest regarding the publication of this paper.

Acknowledgments

This study was supported by the National Natural Science Foundation of China under grant no. 51305139. The authors give sincere thanks to Ze-Biao Yang and Jie Huang for doing experiments.

References

[1] K. Shah and S. B. Choi, "The influence of particle size on the rheological properties of plate-like iron particle based magnetorheological fluids," *Smart Materials and Structures*, vol. 24, no. 1, Article ID 015004, 2015.

[2] J. D. Carlson and M. R. Jolly, "MR fluids, foam and elastomer device," *Mechatronic*, vol. 10, pp. 555–569, 2001.

[3] D. J. Klingenberg, "Magnetorheology: applications and challenges," *AIChE Journal*, vol. 47, no. 2, pp. 246–249, 2001.

[4] D. Guo and H. Hu, "Nonlinear stiffness of a magneto-rheological damper," *Nonlinear Dynamics*, vol. 40, no. 3, pp. 241–249, 2005.

[5] S.-J. Moon, Y.-C. Huh, H.-J. Jung, D.-D. Jang, and H.-J. Lee, "Sub-optimal design procedure of valve-mode magneto-rheological fluid dampers for structural control," *KSCE Journal of Civil Engineering*, vol. 15, no. 5, pp. 867–873, 2011.

[6] W. W. Chooi and S. O. Oyadiji, "Design, modelling and testing of magnetorheological (MR) dampers using analytical flow solutions," *Computers and Structures*, vol. 86, no. 3–5, pp. 473–482, 2008.

[7] Y.-H. Zeng, S.-J. Liu, and J.-Q. E, "Neuron PI control for semi-active suspension system of tracked vehicle," *Journal of Central South University*, vol. 18, no. 2, pp. 444–450, 2011.

[8] S. J. Dyke, B. F. Spencer, M. K. Sain, and J. D. Carlson, "An experimental study of MR dampers for seismic protection," *Smart Materials and Structures*, vol. 7, no. 5, pp. 693–703, 1998.

[9] M. Zapateiro, H. R. Karimi, N. Luo, and B. F. Spencer, "Real-time hybrid testing of semi-active control strategies for vibration reduction in a structure with MR damper," *Structural Control and Health Monitoring*, vol. 17, pp. 427–451, 2010.

[10] F. Weber, "Semi-active vibration absorber based on real-time controlled MR damper," *Mechanical Systems and Signal Processing*, vol. 46, no. 2, pp. 272–288, 2014.

[11] https://www.bwigroup.com/.

[12] X. X. Bai, N. M. Wereley, and W. Hu, "Maximizing semi-active vibration isolation utilizing a magneto-rheological damper with an inner bypass configuration," *Journal of Applied Physics*, vol. 117, no. 17, Article ID 17C711, 2015.

[13] X. J. Yuan, T. Y. Tian, H. T. Ling et al., "A review on structural development of magneto-rheological fluid damper," *Shock and Vibration*, vol. 2019, Article ID 1498962, 33 pages, 2019.

[14] X. Song, M. Ahmadian, and S. Southward, "Analysis and strategy for superharmonics with semiactive suspension control systems," *Journal of Dynamic Systems, Measurement, and Control*, vol. 129, no. 6, pp. 795–803, 2007.

[15] U. Dogruer, F. Gordaninejad, and C. A. Evrensel, "A new magnetorheological fluid damper for high-mobility multi-purpose wheeled vehicle (HMMWV)," *Journal of Intelligent Material Systems and Structures*, vol. 19, no. 6, pp. 641–650, 2007.

[16] X. Dong, M. Yu, and Z. Guan, "Adaptive sliding mode fault-tolerant control for semi-active suspension using magneto-rheological dampers," *Journal of Intelligent Material Systems and Structures*, vol. 22, no. 15, pp. 1653–1660, 2011.

[17] M. Zapateiro, F. Pozo, H. R. Karimi, and N. Luo, "Semiactive control methodologies for suspension control with magnetorheological dampers," *IEEE/ASME Transactions on Mechatronics*, vol. 17, no. 2, pp. 370–380, 2012.
[18] R. T. Foister, T. W. Nehl, W. C. Kruckemeyer et al., "Magnetorheological (MR) piston assembly with primary and secondary channels to improve MR damper force," US Patent 8327984 B2, 2011.
[19] J. W. Sohn, J. S. Oh, and S. B. Choi, "Design and novel type of a magneto-rheological damper featuring piston bypass hole," *Smart Materials and Structures*, vol. 24, Article ID 035013, 2015.
[20] L. Guojie, "Simulation of Damping Force for a Magneto-Rheological (MR) Damper Featuring Piston Bypass Holes," in *Proceedings of the SAE Technical Paper Grand Rapids*, MI, USA, June 2019.
[21] N. M. Wereley, Y.-T. Choi, and H. J. Singh, "Adaptive energy absorbers for drop-induced shock mitigation," *Journal of Intelligent Material Systems and Structures*, vol. 22, no. 6, pp. 515–519, 2011.
[22] M. Mao, W. Hu, Y. T. Choi, N. Wereley, A. L. Browne, and J. Ulicny, "Experimental validation of a magnetorheological energy absorber design analysis," *Journal of Intelligent Material Systems and Structures*, vol. 25, no. 3, pp. 352–363, 2014.
[23] M. Mao, W. Hu, Y.-T. Choi, and N. M. Wereley, "A magnetorheological damper with bifold valves for shock and vibration mitigation," *Journal of Intelligent Material Systems and Structures*, vol. 18, no. 12, pp. 1227–1232, 2007.
[24] H. J. Singh and N. M. Wereley, "Optimal control of gun recoil in direct fire using magnetorheological absorbers," *Smart Materials and Structures*, vol. 23, no. 5, Article ID 055009, 2014.
[25] B. E. Powers, N. M. Wereley, and Y. T. Choi, "Analysis of impact loads in a magnetorheological energy absorber using a Bingham plastic model with refined minor loss factors accounting for turbulent transition," *Meccanica*, vol. 51, no. 12, pp. 3043–3054, 2016.
[26] https://www.lord.com.
[27] J. D. Carlson, "MR fluids and devices in the real world," *International Journal of Modern Physics B*, vol. 19, no. 7–9, pp. 1463–1470, 2005.